Biodegradation of Functionalized Nanocellulose

Benjamin P. Frank[1], Casey Smith[1], Emily R. Caudill[2], Ronald S. Lankone[1], Katrina Carlin[1], Sarah Benware,[2] Joel A. Pedersen[2,3], D. Howard Fairbrother[1*]

[1]Department of Chemistry, Johns Hopkins University, 3400 N Charles Street, Baltimore, MD 21218, United States

[2]Department of Chemistry, University of Wisconsin-Madison, 1101 University Avenue, Madison, Wisconsin 53706, United States

[3]Departments of Soil Science and Civil & Environmental Engineering, University of Wisconsin-Madison, 1525 Observatory Drive, Madison, WI, 53706, USA

*Corresponding Author

Email: howardf@jhu.edu

Address: Department of Chemistry, 3400 North Charles Street, Baltimore, MD 21218

Keywords: Anaerobic digestion, surface chemistry, nanoparticle, biomethane potential tests, esterification, modified Gompertz model, degree of substitution

Abstract: Nanocellulose has attracted widespread interest for applications in materials science and biomedical engineering due to its natural abundance, desirable physicochemical properties, and ease of mineralization (i.e., complete biodegradation). A common strategy to increase dispersibility in polymer matrices is to modify the hydroxyl groups on nanocellulose through covalent functionalization, but such modification strategies may affect the desirable biodegradation properties exhibited by pristine nanocellulose. In this work, cellulose nanofibrils (CNFs) functionalized with a range of esters, carboxylic acids, or ethers exhibited decreased rates and extents of mineralization by anaerobic and aerobic microbial communities compared to unmodified CNFs, with etherified CNFs exhibiting the highest level of recalcitrance. The decreased biodegradability of functionalized CNFs depended primarily on the degree of substitution at the surface of the material rather than within the bulk. This dependence on surface chemistry was attributed not only to the large surface area-to-volume ratio of nanocellulose, but also to the prerequisite surface interaction by microorganisms necessary to achieve biodegradation. Results from this study highlight the need to quantify the type and coverage of surface substituents in order to anticipate their effects on the environmental persistence of functionalized nanocellulose.

.

Synopsis: This study demonstrated that the microbial biodegradation and environmental persistence of functionalized nanocellulose will be strongly influenced by the type and degree of surface functionalization with bulk functionalization playing a secondary role.

Introduction

Nanocellulose, a naturally occurring biopolymer consisting of β-1,4-D-anhydroglucopyranose monomer units,[1] is derived from macrocellulose via chemical treatment,[2] sonication,[3] mechanical milling,[4] or enzymatic digestion.[5] Nanocellulose possesses desirable mechanical properties (e.g., Young's modulus, tensile strength) comparable to Kevlar and steel.[6, 7] These mechanical properties, along with the nanoscale width, natural abundance, biodegradability, and biocompatibility of nanocellulose, elevate its use in a variety of applications, including polymer nanocomposites,[1, 2, 8] biomedicine,[9] sensors,[9, 10] water treatment,[9, 11] coatings,[12] and smart materials.[13-15] Many applications of nanocellulose require hydrophobic surface modification (e.g., coating, functionalization) to improve its dispersion in organic media and reduce hydrogen bond-induced homoaggregation prior to use in material applications.[10, 16-18] Roughly 35 million tons of nanocellulose are produced globally each year, and production is projected to further increase by 2030.[19, 20] Release of nanocellulose composite materials into the environment is therefore inevitable, necessitating understanding the effect of surface modification on its microbial mineralization.

Products featuring cellulosic materials often advertise the complete biodegradability (i.e., mineralization of carbon into CO_2 and/or CH_4) of cellulose as an attractive feature compared to traditional carbon-based reinforcement options such as carbon nanotubes and carbon fibers due to reduced environmental persistence and impact.[21-24] The biodegradation of cellulosic materials proceeds through different mechanisms and microorganisms in anaerobic and aerobic environments. Specifically, in aerobic environments, cellulose is generally degraded by cellulase and β-glucosidase enzymes secreted by bacteria and fungi. Cellulases initiate degradation of the cellulose structure by hydrolyzing internal bonds (endoglucanases) and chain-ends

(cellobiohydrolases) to yield cellobiose molecules.[25] β-Glucosidase then concludes the depolymerization process by converting cellobiose into glucose which is mineralized to CO_2 and water by aerobic microorganisms.[25] In contrast, anaerobic microorganisms utilize cellulosomes or multiprotein complexes of enzymes to mineralize cellulose into water and biogas consisting of CO_2 and CH_4.[25-27] This conversion to biogas is achieved at over 80% efficiency for cellulose, demonstrating the high biodegradability of the material.[28] Furthermore, while a single aerobic microorganism species is sufficient to fully mineralize cellulose (e.g., the fungus *Trichoderma reesei*), multiple anaerobe species are required to work in concert to produce the enzymes necessary for conversion of cellulose to biogas.[26] Examples of bacterial phyla responsible for cellulose degradation include Acidobacteria and Firmicutes.[29, 30]

While native cellulose is readily fully biodegraded (mineralized), hydrophobic modifications have the potential to interfere with the enzymatic degradation of macrocellulose,[31-33] a process which depends on the composition and activity of the microbial community involved (e.g., aerobic vs. anaerobic).[23, 25, 26, 29, 30, 34] In a previous report, we demonstrated that this interference held true for cellulose nanofibrils (CNFs) modified with hydrophobic siloxane coatings, which blocked enzymatic access to nanocellulose and inhibited its anaerobic mineralization.[16] In contrast, covalent functionalization strategies utilizing ether, ester, and urethane linkages avoid the formation of surface coatings, and have been widely applied to macrocellulose and nanocellulose to improve dispersion in organic media and polymers,[35-38] yet their impact on nanocellulose biodegradation has not been previously investigated. Results from previous studies lead to the expectation that for functionalized nanocellulose, the rate limiting step in biodegradation will involve the removal of functional groups (e.g., ester groups by hydrolysis) to regenerate the functionalizing reagent and the hydroxyl groups present in native cellulose.[32, 39-

[41] After this initial cleavage, the biodegradation pathway of functionalized cellulose proceeds through biodegradation of the native cellulosic component and the functionalizing reagent.

The most commonly used metric to express the extent of covalent functionalization of cellulose is the degree of substitution (DS), representing the average number of cellulosic hydroxyl groups functionalized per anhydroglucose monomer unit (DS = 0-3). The conventionally determined DS value represents the extent of functionalization of both the surface and bulk regions of the material and can therefore be regarded as a measure of the overall DS ($DS_{overall}$). For cellulosic materials, the $DS_{overall}$ is generally determined using elemental analysis[42] or nuclear magnetic resonance (NMR) spectroscopy.[43, 44] For covalently modified macrocellulose, biodegradability depends on both $DS_{overall}$ and the nature of the chemical linkage (i.e., ether,[45-47] ester[31, 32, 48]). For example, degradation of macrocellulose fibers functionalized with carboxymethyl groups (ether linkage) by a cellulolytic enzyme complex decreased as the $DS_{overall}$ increased from 0.41 to 1.30.[46] Furthermore, nanocellulose esterified with acetyl groups to $DS_{overall}$ >1.25 exhibited significant inhibition of anaerobic biodegradation as compared to un-modified macrocellulose.[48]

Past studies typically quantified the extent of modified macrocellulose biodegradation in terms of the production of low molecular mass byproducts (e.g., cellobiose, glycolic acid) rather than evolution of CO_2 or CH_4. Furthermore, many studies on modified macrocellulose employed model enzymes (e.g., cellulase, esterase) or a single microbial species to effect biodegradation.[46, 47, 49] While the information from these studies is useful in identifying trends in biodegradation as a function of material properties, such approaches do not measure complete biodegradation of the cellulosic material and do not represent the microbial communities encountered in natural environments.[23, 24, 34, 46, 47, 49] Failure to discern the complete mineralization of functionalized

cellulose has led to disagreement with respect to the degree of inhibition resulting from chemical functionalization.[31, 33, 45] Additionally, as mineralization of cellulosic materials generally proceeds via the cooperation of a microbial community,[27] more complex systems utilizing environmentally relevant microorganisms are best suited for assessing the environmental persistence of functionalized nanocellulose, rather than model enzymes or pure microbial cultures.[23, 34] One established method of measuring the anaerobic biodegradation of cellulose involves the quantification of biogas produced during the mineralization of carbon into CO_2 and CH_4.[28, 31, 48, 50] The aerobic biodegradation of cellulose is typically quantified using mass loss measurements to compare the amount of carbon converted from the solid (i.e., cellulosic) phase into the gas phase (i.e., CO_2).[31, 51, 52]

Another potentially important factor to consider is that the extent to which the biodegradation of a functionalized nanomaterial is inhibited may be more closely linked to the degree of functionalization of the surface ($DS_{surface}$) than to $DS_{overall}$. This distinction is important as the preliminary step in the biodegradation of a solid-phase material involves the adsorption and colonization of microorganisms at the surface.[53-56] In the case of cellulosic materials, this initial biodegradation step requires biofilm formation or the interaction of highly specific microbe-secreted cellulosome complexes with its surface.[26, 57-59] As nanocellulose fibers are composed of numerous cellulose chains woven together into a nano-scale cord, the chains at the fiber surface are distinct from those within the bulk of the material.[2, 60, 61] During chemical functionalization with liquid reagents, cellulose chains in both the bulk and surface of nanocellulose are targeted,[2, 62, 63] while gas phase reagents selectively functionalize the nanocellulose surface due to their inability to penetrate into the bulk of the material.[64-66] Despite the potential for achieving different levels of surface vs. bulk functionalization, studies of cellulosic materials typically use only bulk-

144 sensitive analytical techniques (e.g., NMR), and thus quantify only $DS_{overall}$.[42, 44, 67-70] The effect of
145 surface substitution is likely to be particularly important for the biodegradation of CNFs compared
146 to macrocellulose due to the large surface area-to-volume ratio of nanocellulose as well as the
147 decreased swelling capacity of CNFs which limits access to bulk cellulose chains.[2]

148 In this study, we compare the influence of surface vs. bulk functionalization as well as the
149 influence of different covalent linkages on CNF mineralization by aerobic and anaerobic microbial
150 communities. This study is the first to investigate the biodegradability of a range of functionalized
151 nanocellulose in both aerobic and anaerobic environments. Selective functionalization of the
152 surface and bulk regions was accomplished using liquid-phase and gas-phase (i.e., surface-
153 specific)[64, 65] techniques to esterify nanocellulose with long-chain hydrocarbons that are often used
154 to improve CNF dispersion in polymer nanocomposites.[63, 71] Attenuated total internal reflectance
155 Fourier-transform infrared spectroscopy (ATR-FTIR), solid-state ^{13}C-nuclear magnetic resonance
156 spectroscopy (^{13}C-NMR), and CHN elemental analysis were used to confirm functionalization.
157 Elemental analysis was used to determine $DS_{overall}$, while X-ray photoelectron spectroscopy (XPS)
158 was utilized to measure $DS_{surface}$.[72] To assess the effect of different covalent linkages, CNFs were
159 functionalized with different esters (phenyl, hexyl, dodecyl) and ethers (hexyl, dodecyl), which
160 were also compared to common TEMPO oxidized nanocellulose carboxylates with H^+ or Na^+
161 counterions. Biodegradation of these samples by anaerobic and aerobic microorganisms was
162 assessed via biomethane potential (BMP) tests and mass loss, respectively. Results from our study
163 reveal the importance of materials characterization, particularly the surface coverage of added
164 functional groups, in understanding the biodegradation behavior of functionalized CNFs.

Experimental

Functionalization of CNFs. Freeze-dried cellulose nanofibrils (CNFs) were purchased from the University of Maine Process Development Center and either used as-received or milled into a powder with a Flack-tek mill (DAC 150, 2800 rpm, 4 min). Ethyl cellulose (48.0/48.5 % w/w ethoxyl basis) was purchased from Sigma-Aldrich. Carboxylated CNFs were purchased from the University of Maine Process Development Center as a slurry of TEMPO-oxidized CNFs (1 wt% CNF, 1.5 mmol COOH/g cellulose) and dried either as-received (Na^+ counterion) or after washing with dilute HCl (H^+ counterion).

Esterified CNFs were prepared by liquid-phase reactions with carboxylic acid reagents,[73] or with acyl chloride reagents.[63] CNF functionalization with carboxylic acids was performed by dispersing 200 mg of CNFs in 200 mL deionized water followed by a 2 h sonication before adjusting to approximately pH 4 with 4 M HCl. The mixture was then heated to evaporate water followed by addition of excess phenyl acetic acid (phenyl ester CNF), hexanoic acid (hexyl ester CNF), or dodecanoic acid (dodecyl ester CNF, DA-CNF) before melting at ~140 °C to form the reaction medium. Sample solutions were stirred with a magnetic stirrer for 14 h and subsequently quenched with ethanol (Pharmco, 200 proof ACS/USP grade). Functionalized CNF powders were recovered via vacuum filtration, washed with ethanol, and dried in a vacuum oven at 60 °C for 12 h.

Liquid-phase esterification reactions using acyl chlorides were carried out using a modified method derived from literature by dispersing 200 mg of CNFs in 12 mL of diethyl ether and 0.5 mL of triethylamine in a vented round bottom flask equipped with a magnetic stirrer.[63] After dropwise addition of 1 mL of lauroyl chloride, samples were gently mixed at room temperature for 6 h. At the end of the reaction time, samples were quenched with 30 mL of deionized water and recovered

by vacuum filtration followed by a dilute HCl (100 mL, pH 5.5) and a deionized water (800 mL) wash. Samples were then dried in a vacuum oven at 50 °C for 72 h to yield lauroyl chloride esterified CNFs (LC-CNF).

Gas-phase (GP) esterification was performed by adding ~10 mg of CNF powder to a custom-designed Schlenk line vessel[74] suspended above 1 mL of either lauroyl chloride (GP-LC-CNF) or hexanoyl chloride (GP-HC-CNF). The bottom of the vessel was submerged in liquid nitrogen to freeze the reagent, followed by headspace evacuation. After sealing the vessel, the reagent was allowed to thaw and vaporize into the headspace of the vessel to react with the CNF powder.

Etherification was performed by swelling 200 mg of dried CNF in 200 mL of dimethyl sulfoxide (DMSO, Fisher, 99.9%) via sonication for 3 h. After swelling, 200 mg K_2CO_3 (Aldrich, 99.99%) was then added, and the sample sonicated for an additional 3 h. A 30 mL aliquot of 1-bromohexane (hexyl ether CNF; Aldrich, 98%) or 1-bromododecane (dodecyl ether CNF; Aldrich, 97%) was added to the sample before heating to 90 °C and magnetically stirring for 45 min under reflux.[75] The reaction was then quenched with ethanol and the functionalized CNF powder recovered via vacuum filtration followed by thorough washing with ~1 L of ethanol (Pharmco, 200 proof ACS/USP grade) before being dried in a vacuum oven at 60 °C for 12 h.

CNF Characterization. Cellulose nanofibril characterization techniques are briefly described, with complete details in the SI. Functional groups in the unmodified and functionalized CNFs were identified using ATR-FTIR; the bonding and concentrations of C and O at the surface of the unmodified and functionalized CNFs were assessed using XPS; the carbon structure of the nanocellulose before and after functionalization was evaluated via solid-state ^{13}C-NMR; the wt% C, N, O, and H of unmodified and functionalized CNFs was determined by elemental analysis.

Degree of Substitution (DS) Calculations. *DS from Elemental Analysis.* For CNFs functionalized with esters and ethers DS values were calculated from the wt % carbon (Table S1) relative to unmodified CNF ($C_6H_{10}O_5$)[44, 73, 76] with an uncertainty of approximately 0.3 %.[77] For example, an increase in carbon content to 53.0 wt % after esterification with dodecanoic acid ($C_{12}H_{24}O_2$) reflects a DS of 0.45, which corresponds to an average addition of approximately one dodecyl ester group per two glucose monomer units. Because elemental analysis measures the degree of CNF functionalization from the entirety of the sample, DS values determined from elemental analysis are hereafter referred to as $DS_{overall}$.

$DS_{overall}$ of TEMPO CNF. The TEMPO CNF obtained from University of Maine Process Development Center was listed as having 1.5 mmol COOH/g cellulose. Each gram of cellulose features roughly 6.2 mmol of glucose monomer units, which corresponds to 0.243 COOH groups per cellulose unit (1.5 mmol COOH/6.2 mmol cellulose), representing a $DS_{overall}$ of 0.24.

DS from XPS. Degree of substitution values determined by XPS for CNF esters and ethers were based on the fitted contribution from the C–C component (285.0 eV) to the C(1s) XPS envelope. As the C–C content in unmodified CNF was 14.5 ± 3% (due to adventitious carbon), any increase was assumed to be due to functionalization of the nanocellulose surface by ethers or esters. For example, upon esterification with dodecyl ester groups, an increase in the C–C component to 48% would require an average addition of approximately 1 dodecyl ester group per 7 glucose monomer units, corresponding to a DS of 0.43. Since DS values determined by XPS are surface specific and represent the degree of CNF functionalization within only the topmost 2 nm to 3 nm of the sample, they are hereafter referred to as $DS_{surface}$ (Table S2).

DS for Gas-Phase CNF Samples. We estimated the degree of substitution for gas-phase CNF samples (GP-HC-CNF and GP-LC-CNF) from a combination of CHN analysis data and

ATR-FTIR spectra. Due to the low sample mass attainable from gas phase functionalization, we were not able to measure CHN on the full set of samples. Instead, the elemental composition of one sample from each set (GP-HC-CNF-4 and GP-LC-CNF-4) was determined, and the $DS_{overall}$ calculated as described above. The $DS_{overall}$ values of GP-HC-CNF-4 and GP-LC-CNF-4 were then ratioed to the C=O (ester) : C–O (cellulose) peak intensities obtained from ATR-FTIR analysis. As detailed in the results and discussion section, this provided a means to convert the C=O : C–O peak intensities measured on the remaining samples in the two series (GP-HC-CNF and GP-LC-CNF) into their respective $DS_{overall}$ values.

Anaerobic Biodegradation of CNFs. *Biomethane Potential (BMP) Tests.* Mineralization was assessed using biomethane potential tests, adapted with minor modifications from Owen et al.,[50, 78] to monitor biogas (CO_2 and CH_4) production after unmodified and functionalized CNFs were incubated with an anaerobic microbial community. Microbial BMP media (Table S3) was prepared as previously described[16] and heated at 100 °C for 30 min while sparging with N_2 to achieve anoxic conditions before adding anaerobic digestor sludge (10% v/v) obtained from Back River Wastewater Treatment Plant (Baltimore, MD). The BMP media was adjusted to pH ~7 using 20% CO_2 gas and kept anoxic via continuous N_2 sparging. Duplicate 100 mg or 150 mg (DA-CNF only, due to increased sample availability) functionalized CNF samples were mixed with 100 mL of anaerobic media in 150 mL serum bottles and capped with rubber septa. We also assessed 150 mg of each functionalizing reagent (e.g., dodecanoic acid, hexanoic acid) independently to determine their biogas production potential. Samples were incubated at mesophilic temperature (35 °C) for up to 424 d, and biogas production was volumetrically assessed via intermittent headspace measurements with a glass syringe. In each set of samples, blank controls (i.e., anaerobic media including the same concentration of sludge in the absence of a CNF sample) were

incubated in triplicate to account for biogas produced by the residual organic matter in the media (< 10% total solids, ~55% volatile solids before dilution to 10% of media volume).[79-81] Separate control studies were performed with the native (i.e., unfunctionalized) CNF to determine the extent of biogas production in the absence of functionalization and to confirm that the overwhelming majority of CNFs biodegrade to liberate biogas. Importantly, the carbon contributed by cellulose in each sample (42 mg C per 100 mg unfunctionalized CNF, more for functionalized CNF) vastly outweighed the contributed carbon from the BMP media (< 5 mg C in nutrients, most of which is not mineralized). Given the well-known propensity of cellulose to form biogas during biodegradation, the biogas produced by CNF samples was dominated by CNF mineralization. To account for biogas produced from the BMP media, the biogas production from CNF samples at each timepoint was reported as the difference between the volume produced by the CNF sample (typically yielded > 5 mL at each time point) and the average volume of biogas produced from the blank media (< 3 mL per timepoint). In this way, any biogas contribution from the media is removed and the reported biogas data arises solely from the mineralization of the CNF sample. All biogas values were normalized to account for differences in sample mass (comparison between biogas production from 100 mg and 150 mg CNF; Figure S1).

Biodegradation of CNFs in our BMP tests lead predominantly to biogas formation over the course of a few weeks, producing between 680-700 mL/g of biogas, representing over 80% CNF mass loss. This is consistent with the rapid and extensive mineralization of cellulosic materials typically observed.[28, 82] Despite the efficiency of biogas production during CNF biodegradation, some of the carbon is converted into biomass, as is typical of biodegradation processes. This situation also holds true for functionalized CNFs.

The biodegradation of functionalized CNFs proceeds via the hydrolytic cleavage of the

linkage formed between the functional group and the cellulosic monomer, and the subsequent biodegradation of the species generated in this step. For example, in the case of the CNFs functionalized with acyl chlorides, the process will be initiated by the generation of the native CNFs and carboxylic acids, followed by their subsequent biodegradation. For each functionalized CNF, we therefore performed independent biodegradation studies to determine the partitioning between biogas and biomass production for each component, after subtraction of the small amount of biogas produced due to residual carbon and biomass present in the media itself (determined in separate control studies). This information enabled us to determine the biogas each component would generate in the case of complete biodegradation under our experimental conditions. Combined with knowledge of the chemical composition of each functionalized CNF, we could then determine the biogas we would predict in the event of complete biodegradation. For example, a CNF functionalized with a dodecyl ester with a $DS_{overall}$ of 0.45 would be composed of roughly 66 wt % CNF and 34 wt % dodecyl ester. The total biogas produced from this functionalized CNF in the event of complete (100% biodegradation) is expected to be $0.66x + 0.34y$, where x and y are the per gram biogas production potentials of cellulose (680 mL g^{-1}) and dodecanoic acid (1280 mL g^{-1}), respectively (Figure S2). This equates production of 883 mL/g biogas, considerably more than produced from cellulose alone (i.e., 680 mL/g). This predicted value was nearly met for DA-CNF-2 (94% of calculated biogas production was achieved), providing evidence for almost complete biodegradation of this sample, thereby also providing support for the validity of this normalization strategy in computing biogas potentials. By reporting data in these normalized terms (i.e., experimental data/calculated maximum data), we were able to compare samples in terms of their ability to achieve "maximum" biodegradation (a normalized V_{max} value of 1). Explicitly, this value represents the extent to which each functionalized CNF reaches its maximum biogas production

based on the overall partitioning predicted for biogas and biomass production from the components. The biogas values that would be produced in the event of 100% mineralization along with the experimentally measured (empirical) biogas produced for CNFs and all of the functionalized CNFs used in this study are reported in Table S4.

Gompertz Modeling. Anaerobic biogas production rates were quantified using the modified Gompertz kinetic model (Eq. 1)[83-85]

$$V_i = V_{max} e^{-e^{\left(\frac{K*e(\lambda - t_i)}{V_{max}} + 1\right)}} \quad \text{(Eq. 1)}$$

where V_{max} is the experimental ultimate biogas yield (mL g^{-1}), K is the maximum specific rate constant (mL g^{-1} d^{-1}), λ is the lag phase time constant (d), and t_i is the total incubation time (d). The Solver optimization tool in Microsoft Excel was used to estimate the model parameters for each sample by minimizing the root mean square deviations (RMSE, Table S5), and the agreement between predicted and experimental values was evaluated by comparing the RMSE and R^2 values.

Aerobic Biodegradation Tests. Aerobic biodegradation of CNF samples was assessed by measuring mass loss after exposure to an aerobic microbial community obtained from the primary effluent of the Back River Wastewater Treatment Plant (Baltimore, MD). Mass loss was used as the metric for aerobic biodegradation as an open system was required to maintain an oxygenated environment. Triplicate 50 mg samples of CNF powders were sedimented via centrifugation in conical vials (Figure S3) containing an aqueous medium composed of 200 mg/L sodium acetate trihydrate and 10% v/v salt stock (7.18 mM K_2HPO_4, 2.79 mM KH_2PO_4, 0.757 mM $(NH_4)_2SO_4$, 0.0406 mM $MgSO_4 \cdot 7H_2O$), and trace elements necessary for bacterial growth. Microbial media was made by adding 10% v/v primary effluent supernatant to the vials and shaking at 125 rpm at 28 °C for 60 d. These samples were then incubated for 60 days before the powders were recovered

from the media, washed with ultrapure water (18.2 MΩ·cm, Millipore, USA), washed three times with ethanol to remove any adhered biomass/biofilm and then dried in a vacuum oven at 60 °C for 12 h to evaporate any adsorbed water, before being weighed. This approach is analogous to the one used in other aerobic biodegradation studies of cellulosic materials.[28, 51, 52] To account for any native material which was dispersed or otherwise lost in the media, an identical set of samples was incubated for 60 days in uninoculated media and the mass loss observed in these control studies was subtracted from the biotic mass loss values. Consistent with our expectations, the mass loss experienced by the native CNF samples was reproducible and close (80%) to the mass of the CNF added, supporting the idea that comparisons between the extent of mass loss produced by different samples could serve as the basis to compare the extent of biodegradation amongst our functionalized CNF samples. Furthermore, the products of incomplete CNF biodegradation (i.e., cellulose hydrolysis without complete conversion to CO_2) such as cellobiose and glucose monomer units are water soluble and would therefore contribute to the observed mass loss.[86] Thus, the final mass measured in our studies should be composed predominately of undegraded CNF or functionalized CNF samples, as intended. The mass loss for each sample was determined by the difference between the average mass lost in bacterial culture minus the average mass lost in the abiotic media. This difference was then ratioed to the initial mass (50mg) to determine the adjusted % mass loss reported in Figure 1.

In the present investigation, mass loss data from aerobic biodegradation studies was used as a semi-quantitative measure of biodegradation amongst functionalized CNFs. Unlike the BMP tests, mass loss was determined at a single time point, precluding application of the modified Gompertz model. Moreover, in the aerobic studies we did not directly assess the mass loss that would accompany the biodegradation of the added functional groups, although the influence of

this unknown is not expected to impact the qualitative conclusions drawn from these studies.

Results and Discussion

CNF naming convention: CNFs were functionalized with different ester, carboxylic acid, and ether groups (Figure S4, S5). CNF ethers functionalized using 1-bromohexane and 1-bromododecane are referred to as hexyl ether CNF and dodecyl ether CNF, respectively. CNFs functionalized using phenyl acetic acid, hexanoic acid, and dodecanoic acid (DA) are referred to as phenyl, hexyl, and dodecyl ester CNF, respectively. Samples functionalized with liquid-phase DA are referred to as DA-CNF-X, where X represents the relative $DS_{surface}$ rank in that sample series. For example, DA-CNF-4 represents a CNF functionalized with liquid phase DA at the highest $DS_{surface}$ value of the four samples within the series.[87] Similarly, CNFs functionalized with liquid phase lauroyl chloride (LC) are referred to as LC-CNF-X, and follow the same naming convention. Functionalizations achieved using gas-phase (GP) acyl chlorides are denoted by a GP naming scheme. For example, the CNF with the surface most extensively functionalized by gas phase hexanoyl chloride (HC) in a series of four is labeled GP-HC-CNF-4.

Figure 1a shows that unmodified CNFs were completely mineralized after 60 d (Figures 1a and S6) by an anaerobic microbial community. In subsequent discussion, the extent of biodegradation will be expressed relative to (calculated) full mineralization of the sample, unless otherwise noted. Among the three esterified CNFs, the hexyl esterified CNF ($DS_{overall}$: 0.09) exhibited a biodegradation rate comparable to unmodified CNF, while dodecyl ($DS_{overall}$: 0.45) and phenyl ($DS_{overall}$: 0.14) esterified CNFs displayed considerably slower biodegradation rates (Figure 1b), although all three esters were almost completely biodegraded (> 90%) over 424 d (Eq. 1, Table S5). TEMPO-oxidized CNFs containing carboxylate groups with Na^+ and H^+ (Figure S6)

counterions ($DS_{overall}$: 0.24) also biodegraded at markedly slower rates, but ultimately underwent almost complete biodegradation analogous to the behavior of unmodified CNFs. In contrast, etherified nanocellulose was dramatically less susceptible to mineralization even at extremely low $DS_{overall}$ values, with hexyl ($DS_{overall}$: 0.05) and dodecyl ($DS_{overall}$: 0.11) etherified CNFs only biodegrading to 15% and 10% of the levels exhibited by unmodified CNF, respectively, after 424 d of incubation. Biodegradation of functionalized CNFs by an aerobic microbial community, as found in aerobic wastewater, for 60 d revealed similar trends of functional group-induced inhibition towards biodegradation (Figure 1c, 1d), with unmodified CNFs exhibiting 80 % mass loss, hexyl and phenyl CNF esters and carboxylated CNFs all exhibiting mass loss in excess of 9%, and etherified CNFs exhibiting no measurable mass loss.

In the present study, we have measured the effect of different functionalization strategies on the biodegradation of nanocellulose exposed to the same microbial community, revealing that CNF ethers become non-biodegradable at low DS values (≈0.1), in contrast to the behavior of CNF esters at similar DS values. Qualitatively, the trends observed in the relative inhibition of biodegradation induced by introducing specific functional groups mirror those observed for macrocellulose. For example, previous studies on cellulose functionalized with carboxyl groups have also shown over 50% sample biodegradation in soil burial tests.[88] This behavior that has been attributed to the increased swelling of the cellulosic fiber that occurs upon addition of the hydrophilic carboxylic acid functional groups which facilitates enzymatic ingress into the interior of the cellulosic material.[88, 89] The biodegradability of esterified cellulose observed in this study has also been observed for macrocellulose and has been previously attributed to the susceptibility of ester linkages to enzymatic hydrolysis which regenerates the glucose monomer unit of cellulose.[32, 39, 40, 90] The recalcitrance of ether linkages to biodegradation observed in Figure 1 has

been attributed to their resistance to enzymatic attack/hydrolysis.[32, 41, 91] Indeed, we observed a complete lack of biogas production from ethyl cellulose, a commercial, non-biodegradable, macrocellulose ether that produced no biogas over 424 d (Figure 1a). This recalcitrance to mineralization was found for etherified CNFs with very small $DS_{overall}$ values (≈ 0.1).

During the course of our experiments in anaerobic media, and in contrast to our expectations, we observed that an esterified CNF with relatively high $DS_{overall}$ (dodecyl, $DS_{overall}$ 0.45) biodegraded similarly (Figure 1a) to a CNF ester with significantly lower $DS_{overall}$ (phenyl, $DS_{overall}$ 0.14). Based on existing literature for macrocellulose, a threefold increase in $DS_{overall}$ would be expected to decrease the biodegradability of esterified CNFs by over 90%.[48] These data suggested that conventional $DS_{overall}$ values may not be predictive of the relative biodegradability of functionalized nanocellulose. One possible explanation is that the large surface area-to-volume ratio of nanocellulose causes the surface of functionalized CNFs to take on increased importance relative to macrocellulose. To explore this possibility, a series of esterified CNFs with varying degrees of surface ($DS_{surface}$) and overall ($DS_{overall}$) functionalization was synthesized, characterized, and biodegraded by anaerobic microorganisms where comparisons of biodegradation behavior were made easier by virtue of our ability to track biogas formation as a function of incubation time.

CNFs were functionalized with dodecyl ester groups using liquid-phase dodecanoic acid (DA-CNF; Figure 2a-d) and lauroyl chloride (LC-CNF; Figures S7, S8). Elemental analysis revealed that by varying reaction conditions, functionalized CNFs with a range of $DS_{overall}$ values (Table S1) could be prepared for both sets of CNF esters (DA-CNF and LC-CNF). ATR-FTIR provided spectroscopic evidence of functionalization through the observation of CH_2 (2920 cm^{-1} and 2850 cm^{-1}) and C=O (1700 cm^{-1}) stretching modes (LC-CNF; Figure S7) in addition to the

417 characteristic O–H (3339 cm^{-1}), C–H (2905 cm^{-1}), and C–O (1031 cm^{-1}) stretches of cellulose.
418 Moreover, a linear relationship between the $DS_{overall}$ values obtained from elemental analysis and
419 the C=O (ester):C–O (cellulose) vibrational band ratio of DA-CNFs was observed (Figure 2c),
420 suggesting that ATR-FTIR can serve as a facile, non-destructive alternative to elemental analysis
421 for determining $DS_{overall}$ values of functionalized nanocellulose.

422 Solid-state ^{13}C-NMR qualitatively confirmed the trends in $DS_{overall}$ as shown in Figure 2b
423 (increasing for DA-CNF-4, 3, and 2).. The ^{13}C-NMR spectrum of unmodified CNF consists of
424 peaks between 50 and 110 ppm arising from carbons 1-6 in cellulose (C1-C6, labeled in Figure S9
425 and Table S6) and includes peaks arising from amorphous and crystalline nanocellulose. In
426 addition to these principal cellulose peaks, the spectra of esterified CNF contain ester (180 ppm)
427 and methylene (32, 25, 15 ppm) peaks that increased in intensity with increasing reaction time (in
428 order of DA-CNF sample 1, 4, 3, 2). The NMR spectra reveal a minor increase in crystallinity
429 (39% to 58%) of the esterified CNF samples compared to the unmodified CNF sample (Table S7).
430 This is not expected to significantly contribute to differences in biodegradation, however, as
431 crystalline and non-crystalline nanocellulose exhibit similar biodegradation properties[92] (Figure
432 S10). We calculated $DS_{overall}$ from variable contact time cross polarization–magic-angle spinning
433 experiments for two samples: phenyl ester CNF and DA-CNF-2 (Table S8, Figure S11). Variable
434 contact time experiments and elemental analysis produced the same ranking of $DS_{overall}$. The values
435 of $DS_{overall}$ for the phenyl ester CNF samples were more similar for the two measurements than
436 they were for the DA-CNF-2 samples. Differences in $DS_{overall}$ derived from variable contact time
437 experiments from those determined by elemental analysis are possibly due to multiple $T_{1\rho H}$
438 behavior.

439 X-ray Photoelectron Spectroscopy was used to determine $DS_{surface}$ values. Specifically, the

C(1s) region of unmodified CNF contains C–C, C–O, and O–C–O components with peaks at 285.0 eV, 286.6 eV, and 288.5 eV,[93] respectively (Figures 2d, S8), while the O(1s) region features a single broad peak centered at 533.2 eV. With increased $DS_{surface}$, the C–C component increases in intensity due to the grafting of long alkyl chain ester groups. Importantly, changes in $DS_{surface}$ did not correlate with changes in $DS_{overall}$; for example, DA-CNF-2 features the second lowest $DS_{surface}$ (0.10), but the highest $DS_{overall}$ (0.45). In addition to liquid-phase esterification, gas-phase reactions using lauroyl or hexanoyl chloride were performed with the expectation that this approach would restrict functionalization to the CNF surface (Figure S12). The XPS spectra in Figure S12 confirms that measurable increases in $DS_{surface}$ occurred after gas-phase CNF functionalization in the absence of significant bulk functionalization (Figure S13).

Esterified CNFs functionalized with dodecanoic acid (DA-CNFs) and lauroyl chloride (LC-CNFs) were biodegraded by an anaerobic microbial community (Figures 3 and S14) to assess the sensitivity of CNF biodegradability to changes in $DS_{surface}$, $DS_{overall}$, and/or both. The rate and extent of biodegradation of both CNF types were found to change systematically in response to changes in $DS_{surface}$, but not $DS_{overall}$ (Figure 3, Table S9, Figure S15). This trend is most clearly demonstrated by DA-CNF samples where increases in $DS_{surface}$ led to systematic decreases in biodegradation, while $DS_{overall}$ values did not correlate with biodegradation trends (Figure 3a, Figure S15). As an example, DA-CNF-2 possessed the highest $DS_{overall}$ value (0.45) of the DA-CNFs, and yet was almost completely biodegraded (94%), albeit at a slower (29%) rate compared to unmodified CNFs.

Analogous behavior is observed with LC-CNFs. As the extent of surface functionalization ($DS_{surface}$) increased in LC-CNF samples, the extent and rate of biogas production decreased, with the most extensively surface functionalized CNF in this series (LC-CNF-4) exhibiting a biogas

production rate and extent of biodegradation only 24% and 37% of unmodified CNF, respectively (Figure 3b). The lack of correlation with $DS_{overall}$ is observed most clearly in LC-CNF-3: this sample featured the lowest $DS_{overall}$ (0.56) of the LC-CNFs but was more recalcitrant to biodegradation than LC-CNF-1 and LC-CNF-2, which each featured a $DS_{overall}$ of approximately 0.8 (Figure 3b).

We note that LC-CNF samples experienced more extensive overall biodegradation than DA-CNF samples despite LC-CNF samples reaching higher $DS_{surface}$ values (max 2.46) than DA-CNFs (max 0.43). This behavior is a direct result of the production of HCl during CNF functionalization with acyl chlorides, which reduces cellulose chain length and particle size.[63, 94-97] This decrease in chain length increases the overall biodegradability of cellulosic materials by offering more sites/surface area (e.g., chain ends) for the initiation of enzymatic attack.[55, 98, 99] In contrast, esterification using carboxylic acid reagents as used in the synthesis of DA-CNFs does not produce HCl at the site of functionalization, limiting damage to the cellulose chain, thereby producing DA-CNF samples with lower $DS_{surface}$ values which undergo a smaller degree of biodegradation.

Gas-phase functionalization was used to specifically target the role of surface functionalization in biodegradation. To this end, CNF surfaces were modified with lauroyl chloride (GP-LC-CNF) and hexanoyl chloride (GP-HC-CNF). Hexanoyl chloride enabled a wider range of and higher $DS_{surface}$ values to be achieved (1.19-2.43) compared to lauroyl chloride (0.07-0.33) due to its higher volatility (hexanoyl chloride $T_b \approx 150$ °C vs. lauroyl chloride $T_b \approx 260$ °C). Because these esterified samples exhibited levels of overall substitution (i.e., $DS_{overall} < 0.17$, Figure S13) that would not slow the biodegradation of CNF esters (see Table S9), the effect of surface functionalization on the biodegradation of nanocellulose could be isolated (Figures 3c-d and S14).

The extremely low levels of $DS_{overall}$ produced by gas-phase functionalization compared to the corresponding $DS_{surface}$ values can be appreciated if we consider that the CNFs have diameters ~50 nm and that the XPS measurements of the near-surface region are dominated by photoelectrons from the outermost 3 nm of the CNFs.[100] Thus, even in the event that 100% of the CNF hydroxyl groups in the near-surface region were functionalized (i.e., $DS_{surface}$ of 3.0), the corresponding $DS_{overall}$ would be only approximately 0.2.

The specificity of surface functionalization realized with these gas-phase modified CNF samples provided a clear indication of the role that $DS_{surface}$ plays in regulating CNF biodegradability. As seen in Figure 3c, GP-HC-CNF-1, the least functionalized GP-HC-CNF samples ($DS_{surface}$ 1.19), displayed a 60% reduction in biogas production rate compared to unmodified CNF. In contrast, the most surface functionalized GP-HC-CNF (GP-HC-CNF-4; $DS_{surface}$ 2.43) exhibited a biogas production rate only 17% of that observed for unmodified CNF. The extent of biodegradation followed the same dependence on $DS_{surface}$, with GP-HC-CNF-1 and GP-HC-CNF-4 samples undergoing 100% and 70% biodegradation, respectively. As expected, the CNFs functionalized with gas phase lauroyl chloride were also more recalcitrant to biodegradation (Figure 3d) than unmodified CNF, but less so than GP-HC-CNFs (lower $DS_{surface}$ values). GP-LC-CNF samples with $DS_{surface}$ values > 0.17 exhibited measurable decreases in the biogas production rate (> 40% reduction), although the extent of biodegradation reached approximately 90% of the value expected for unmodified CNFs after 75 d due to the relatively low (< 0.35 $DS_{surface}$) levels of surface functionalization.

Figure 3 reveals that for both gas- and liquid-phase CNF functionalization, the extent and rate of biodegradation decrease with increasing $DS_{surface}$ values, largely independent of $DS_{overall}$ values. This dependency on surface chemistry is consistent with the environmental properties of

509 other carbon nanomaterials such as carbon nanotubes,[101, 102] carbon dots,[103-105] and graphene,[106,
510 107] which have previously been found to be influenced—and in some cases wholly determined—
511 by surface properties. Of significance, the observed reduction in biodegradability for
512 functionalized nanocellulose manifested as a decreased propensity to be mineralized into biogas
513 (i.e., complete biodegradation). Consequently, either the parent material or products of incomplete
514 biodegradation may persist even in conditions with high microbial activity and result in
515 environmental accumulation.

516 The importance of surface functionalization is likely a reflection of the biodegradation
517 mechanism of cellulosic materials, which is typically initiated at the surface via highly specific
518 interactions with microbial enzymes.[26, 56, 59] For example, during anaerobic biodegradation,
519 cellulose is completely mineralized by microorganisms which initiate the process using
520 extracellular cellulosomes or multiprotein complexes of cellulolytic enzymes.[25-27] These enzymes
521 are particularly sensitive to the surface of the substrate material, and microorganisms alter the
522 structural and enzymatic composition of the cellulosome to suit the substrate in question.[57] The
523 small length of the glucose subunits of cellulose (roughly 0.5 nm)[108] compared to that of
524 cellulosomes (roughly 18 nm)[109] suggests that functional groups covalently attached to surface
525 subunits of nanocellulose, even at low concentrations, must be removed before conventional
526 enzymatic degradation can proceed.[57, 58, 110] Specifically, biodegradation will be delayed until these
527 functionalized surface sites have been sufficiently removed to regenerate a cellulose substrate
528 recognizable to microbial cellulosomes. The surface-dependent hydrolysis of these functionalized
529 sites serves as the rate-limiting step for the biodegradation of functionalized nanocellulose and
530 likely explains why the bulk of the material is of less importance in determining the rate and extent
531 of biodegradation.

For esterified CNFs with relatively low degrees of surface functionalization (e.g., DA-CNF-1, phenyl ester CNF; $DS_{overall} \leq 0.14$), the presence of ester groups at the surface causes a decrease in biodegradation rate—although the CNF still ultimately biodegrades. However, as the degree of surface functionalization increases (e.g., DA-CNF-4, LC-CNF-4), our data indicates that an increasing fraction of the CNFs are recalcitrant to biodegradation (see Figure 3) despite the enzymatic susceptibility of ester groups. We ascribe this effect to the concentrations of ester groups in certain regions of the surface being sufficiently high to interfere with enzyme regioselectivity, blocking esterases from properly orienting with a single ester group and thus preventing their hydrolysis.[90] As the DS value increases, the fraction of the CNF surface covered with sufficiently high concentrations of ester groups to prevent biodegradation increases. This argument is supported by the observation that esterases are unable to biodegrade macrocellulose esters with high DS values[31, 48, 90] The observed inhibitory effect is enhanced when the covalent linkages are resistant to enzymatic hydrolysis, as is the case for etherified CNFs,[91] where a $DS_{surface}$ of 0.16 and 0.25 was sufficient to prevent biodegradation of dodecyl and hexyl ether CNFs, respectively (see Figure 1). Indeed, the larger $DS_{surface}$ vs $DS_{overall}$ values for etherified CNFs (e.g., 0.16 vs. 0.11, respectively for dodecyl ether CNF; see Figure 1b) helps to explain why these functionalized CNFs were so recalcitrant to biodegradation even at low levels of $DS_{overall}$.

In contrast to our findings, $DS_{overall}$ is generally found to be a reasonable predictor for the biodegradation behavior of macrocellulose, with the degree of surface functionalization rarely reported in biodegradation studies.[31, 46-48] One potential explanation for this difference between macro- and nanocellulose is that a stronger correlation between $DS_{overall}$ and $DS_{surface}$ may exist for macrocellulose. In this respect, we note that macrocellulose exhibits an increased swelling capacity (~48% vs. ~26% for macrocellulose compared to CNFs in aqueous media). This will almost

555 certainly increase the ingress of chemical reagents into the interior of macrocellulose during liquid
556 phase functionalization, likely leading to more similar degrees of bulk vs surface functionalization
557 in macrocellulose compared to CNFs.[111-113] Regardless of the detailed mechanistic underpinnings,
558 results from this investigation highlight the need to measure both $DS_{overall}$ and $DS_{surface}$ for
559 functionalized macrocellulose, and to establish the influence of these two metrics on
560 biodegradation properties.

561 **Implications**

562 The increased recalcitrance of surface functionalized nanocellulose to mineralization is
563 undesirable because complete biodegradation is necessary to ensure its removal from the
564 environment, minimizing accumulation and any consequent impact.[23, 24] The present study has
565 revealed that the extent of surface functionalization and type of covalent linkage strongly influence
566 the degree of CNF recalcitrance to biodegradation. We note that the use of microbial communities
567 derived from wastewater represent optimized conditions for the biodegradation of cellulose due to
568 the diversity, activity, and concentration of microorganisms in the culture as well as the availability
569 of nutrients in the BMP tests.[16, 114-116] Therefore, under environmental conditions where less
570 diverse microbial communities exist (e.g., soils, aquatic sediments), the effect of functionalization
571 on nanocellulose mineralization is expected to be more pronounced relative to the effects observed
572 in this study. We note that the primary biological transformation products of functionalized
573 nanocellulose are expected be carbon dioxide and methane in anaerobic environments and carbon
574 dioxide in aerobic environments; both gases contribute to the greenhouse effect. Thus, although
575 biodegradation is typically viewed as a positive environmental outcome because it acts to remove
576 otherwise persistent materials its effects are not without consequences.

We found that although relative biodegradation trends among different functionalized CNFs were independent of the microbial community (i.e., aerobic vs. anaerobic), the magnitude of inhibition differed (Figure 1d). Specifically, the extent of biodegradation was reduced in aerobic wastewater compared to anaerobic wastewater, likely due to differences in microbial population and numbers. The decreased aerobic biodegradation of functionalized CNF suggests that anaerobic digestion should be utilized to maximize biodegradation of functionalized CNFs and reduce landfill disposal.

While sustainability has been identified as an area of focus in the production phase of surface-modified nanocellulose,[64, 73, 117] the end-of-life environmental fate of such nanomaterials has been largely overlooked or assumed to be comparable to unmodified nanocellulose.[1, 21, 118-120] Importantly, products which utilize surface-functionalized nanocellulose and are marketed as biodegradable (e.g., packaging materials)[21, 121] may actually feature environmentally persistent nanocellulose. For example, the combination of surface-esterified nanocellulose with the biodegradable polymer poly(3-hydroxybutyrate-*co*-3-hydroxyvalerate) (PHBV) to create a strengthened material deemed appropriate for use as a fully biodegradable food packaging material.[21] However, based on our data, the surface-level esterification of nanocellulose used in the reinforcement of PHBV would significantly reduce its overall biodegradability. The same argument holds true for functionalized nanocellulose used in other applications such as in displays and coatings.[12, 122-125] For example, Granström et al., developed a stearoyl ester CNF-based aerogel with projected applications in coatings and insulators[12] that our study indicates will not biodegrade as rapidly as unmodified nanocellulose. Indeed, applications of esterified CNFs in packaging materials, coatings, and lubricants are expected to spur a growth in production to meet increased demand.[21, 62, 121, 122, 126] Our study highlights that the commercial benefit achieved through

functionalization of nanocellulose must be carefully weighed against the consequent changes in the persistence of these nanomaterials. For example, decreasing the cellulose chain length and DS for CNFs functionalized with esters can be anticipated to increase biodegradability, but by the same token these changes are also likely to decrease CNF dispersibility in organic solvents with potential impacts on materials properties. Another practical consequence of the findings from this study is that even relatively low degrees of CNF surface functionalization lead to a portion of the material becoming recalcitrant to biodegradation. Moreover, due to the differential influence of $DS_{surface}$ and $DS_{overall}$ on the biodegradation of functionalized CNF direct comparisons of the effects that different functional groups play in mediating CNF biodegradation is difficult because both $DS_{overall}$ and $DS_{surface}$ need to be similar to isolate the impact of different functional groups on the biodegradation of the functionalized CNF. However, due to the difference in bulk vs. surface accessibility and reagent reactivity, exerting control over these two parameters experimentally is difficult.

Supporting Information

Detailed information about instrumental parameters for material characterization (CHN analysis, ATR-FTIR, XPS, NMR). Specific information on solid state NMR experiments, theory, and data (e.g., crystallinity and peak positions). Tables listing $DS_{overall}$ and $DS_{surface}$ values with corresponding CHN and XPS data for all samples. Comparison of calculated maximum biogas production to empirical biogas production volume. Biogas production curves for CNF and functionalization reagents which enabled comparison of biodegradation from different functionalized CNFs. Gompertz model parameters for kinetic modeling of biogas production curves. Complete ATR-FTIR and XPS spectra for samples examined in the study. Unnormalized

biogas production curves for functionalized CNFs. Direct comparison of $DS_{surface}$ and $DS_{overall}$ with maximum biogas production from each sample.

Acknowledgements

This material is based upon work supported by the National Science Foundation under Grant No. CHE-2001611, the NSF Center for Sustainable Nanotechnology (CSN). The CSN is part of the Centers for Chemical Innovation Program. The authors thank Meng Wu and Cathy Murphy (University of Illinois Urbana-Champaign) for assistance in obtaining the elemental analysis data and Cathy Clewett (Chemistry NMR Facility, University of Wisconsin – Madison) for helpful advice. The National Magnetic Resonance Facility at Madison is supported by NIH grants P41 GM103399 (NIGMS) and P41GM66326 (NIGMS). Additional equipment was purchased with funds from the University of Wisconsin, NIH (RR02781, RR08438), NSF (DMB-8415048, OIA-9977486, BIR-9214394), and USDA. The Bruker AVANCE III 500 NMR spectrometer was supported by a UW2020 grant and a generous gift from Paul J. and Margaret M. Bender. The authors thank Chris Krout from the Back River Wastewater Treatment Plant (Baltimore, MD) for the microbial samples.

References

1. Kalia, S.; Dufresne, A.; Cherian, B. M.; Kaith, B. S.; Averous, L.; Njuguna, J.; Nassiopoulos, E., Cellulose-Based Bio- and Nanocomposites: A Review. *Int. J. Polym. Sci.* **2011,** *2011*.
2. Dufresne, A., *Nanocellulose: From Nature to High Performance Tailored Materials*. Walter de Gruyter: Berlin, Germany, 2012.
3. Hamid, S. B. A.; Zain, S. K.; Das, R.; Centi, G., Synergic Effect of Tungstophosphoric Acid and Sonication for Rapid Synthesis of Crystalline Nanocellulose. *Carbohydr. Polym.* **2016,** *138*, 349-355.
4. Phanthong, P.; Karnjanakom, S.; Reubroycharoen, P.; Hao, X.; Abudula, A.; Guan, G., A Facile One-Step Way for Extraction of Nanocellulose with High Yield by Ball Milling with Ionic Liquid. *Cellulose* **2017,** *24*, (5), 2083-2093.
5. Henriksson, M.; Henriksson, G.; Berglund, L. A.; Lindström, T., An Environmentally Friendly Method for Enzyme-Assisted Preparation of Microfibrillated Cellulose (MFC) Nanofibers. *Eur. Polym. J.* **2007,** *43*, (8), 3434-3441.
6. Moon, R. J.; Martini, A.; Nairn, J.; Simonsen, J.; Youngblood, J., Cellulose nanomaterials review: structure, properties and nanocomposites. *Chem. Soc. Rev.* **2011,** *40*, (7), 3941-3994.
7. Bharimalla, A. K.; Deshmukh, S. P.; Vigneshwaran, N.; Patil, P. G.; Prasad, V., Nanocellulose-Polymer Composites for Applications in Food Packaging: Current Status, Future Prospects and Challenges. *Polym. Plast. Technol. Eng.* **2017,** *56*, (8), 805-823.
8. Wei, H.; Rodriguez, K.; Renneckar, S.; Vikesland, P. J., Environmental science and engineering applications of nanocellulose-based nanocomposites. *Environ. Sci.: Nano* **2014,** *1*, (4), 302-316.
9. Li, Y.-Y.; Wang, B.; Ma, M.-G.; Wang, B., Review of Recent Development on Preparation, Properties, and Applications of Cellulose-Based Functional Materials. *Int. J. Polym. Sci.* **2018**.
10. Ummartyotin, S.; Manuspiya, H., A critical review on cellulose: From fundamental to an approach on sensor technology. *Renewable and Sustainable Energy Reviews* **2015,** *41*, 402-412.
11. Mohammed, N.; Grishkewich, N.; Tam, K. C., Cellulose nanomaterials: promising sustainable nanomaterials for application in water/wastewater treatment processes. *Environ. Sci.: Nano* **2018,** *5*, (3), 623-658.
12. Granström, M.; née Pääkkö, M. K.; Jin, H.; Kolehmainen, E.; Kilpeläinen, I.; Ikkala, O., Highly water repellent aerogels based on cellulose stearoyl esters. *Polymer Chemistry* **2011,** *2*, (8), 1789-1796.
13. Phanthong, P.; Reubroycharoen, P.; Hao, X.; Xu, G.; Abudula, A.; Guan, G., Nanocellulose: Extraction and application. *Carbon Resources Conversion* **2018,** *1*, (1), 32-43.
14. Qiu, X.; Hu, S., "Smart" Materials Based on Cellulose: A Review of the Preparations, Properties, and Applications. *Materials* **2013,** *6*, (3), 738-781.
15. Nasseri, R.; Deutschman, C. P.; Han, L.; Pope, M. A.; Tam, K. C., Cellulose nanocrystals in smart and stimuli-responsive materials: a review. *Materials Today Advances* **2020,** *5*, 100055.
16. Frank, B. P.; Durkin, D. P.; Caudill, E. R.; Zhu, L.; White, D. H.; Curry, M. L.; Pedersen, J. A.; Fairbrother, D. H., Impact of Silanization on the Structure, Dispersion Properties, and Biodegradability of Nanocellulose as a Nanocomposite Filler. *ACS Applied Nano Materials* **2018,** *1*, (12), 7025-7038.
17. Nakatani, H.; Iwakura, K.; Miyazaki, K.; Okazaki, N.; Terano, M., Effect of Chemical Structure of Silane Coupling Agent on Interface Adhesion Properties of Syndiotactic Polypropylene/Cellulose Composite. *J. Appl. Polym. Sci.* **2011,** *119*, (3), 1732-1741.
18. Chin, K.-M.; Sung Ting, S.; Ong, H. L.; Omar, M., Surface functionalized nanocellulose as a veritable inclusionary material in contemporary bioinspired applications: A review. *J. Appl. Polym. Sci.* **2018,** *135*, (13), 46065.
19. Brun, V.; Hansen, F.; Turpin, D.; Bennett, K., Cellulose Nanomaterials Research Roadmap. *Agenda 2020 Technology Alliance* **2016**.
20. Madsen, L. D.; Svedberg, E. B., *Materials Research for Manufacturing: An Industrial Perspective of Turning Materials into New Products*. Springer International Publishing: Switzerland, 2016; Vol. 224.

21. Yu, H.; Yan, C.; Yao, J., Fully biodegradable food packaging materials based on functionalized cellulose nanocrystals/poly(3-hydroxybutyrate-co-3-hydroxyvalerate) nanocomposites. *RSC Adv.* **2014,** *4*, (104), 59792-59802.
22. Carpenter, A. W.; de Lannoy, C. F.; Wiesner, M. R., Cellulose Nanomaterials in Water Treatment Technologies. *Environ. Sci. Technol.* **2015,** *49*, (9), 5277-5287.
23. Zumstein, M. T.; Narayan, R.; Kohler, H.-P. E.; McNeill, K.; Sander, M., Dos and Do Nots When Assessing the Biodegradation of Plastics. *Environ. Sci. Technol.* **2019,** *53*, (17), 9967-9969.
24. Zumstein, M. T.; Schintlmeister, A.; Nelson, T. F.; Baumgartner, R.; Woebken, D.; Wagner, M.; Kohler, H.-P. E.; McNeill, K.; Sander, M., Biodegradation of synthetic polymers in soils: Tracking carbon into CO(2) and microbial biomass. *Sci Adv* **2018,** *4*, (7), eaas9024-eaas9024.
25. Pérez, J.; Muñoz-Dorado, J.; de la Rubia, T.; Martínez, J., Biodegradation and biological treatments of cellulose, hemicellulose and lignin: an overview. *International Microbiology* **2002,** *5*, (2), 53-63.
26. Leschine, S. B., Cellulose Degradation in Anaerobic Environments. *Annu. Rev. Microbiol.* **1995,** *49*, (1), 399-426.
27. Béguin, P.; Aubert, J.-P., The biological degradation of cellulose. *FEMS Microbiology Reviews* **1994,** *13*, (1), 25-58.
28. Filer, J.; Ding, H. H.; Chang, S., Biochemical Methane Potential (BMP) Assay Method for Anaerobic Digestion Research. *Water* **2019,** *11*, (5), 921.
29. Singh, G. Biodegradation of Nanocellulose and Microbial Community Response: Effect of Surface Modification and Morphology. Virginia Polytechnic Institute and State University, Blacksburg, VA, 2015.
30. Singh, G.; Chandoha-Lee, C.; Zhang, W.; Renneckar, S.; Vikesland, P. J.; Pruden, A., Biodegradation of Nanocrystalline Cellulose by Two Environmentally-Relevant Consortia. *Water Res.* **2016,** *104*, 137-146.
31. Puls, J.; Wilson, S. A.; Hölter, D., Degradation of Cellulose Acetate-Based Materials: A Review. *Journal of Polymers and the Environment* **2011,** *19*, (1), 152-165.
32. Reese, E. T., Biological Degradation of Cellulose Derivatives. *Industrial & Engineering Chemistry* **1957,** *49*, (1), 89-93.
33. Sakai, K.; Yamauchi, T.; Nakasu, F.; Ohe, T., Biodegradation of Cellulose Acetate by Neisseria sicca. *Bioscience, Biotechnology, and Biochemistry* **1996,** *60*, (10), 1617-1622.
34. Haider, T. P.; Völker, C.; Kramm, J.; Landfester, K.; Wurm, F. R., Plastics of the Future? The Impact of Biodegradable Polymers on the Environment and on Society. *Angewandte Chemie International Edition* **2019,** *58*, (1), 50-62.
35. Ly, B.; Thielemans, W.; Dufresne, A.; Chaussy, D.; Belgacem, M. N., Surface functionalization of cellulose fibres and their incorporation in renewable polymeric matrices. *Compos. Sci. Technol.* **2008,** *68*, (15), 3193-3201.
36. Jandura, P.; Kokta, B. V.; Riedl, B., Cellulose Fibers/Polyethylene Hybrid Composites: Effect of Long Chain Organic Acid Cellulose Esters and Organic Peroxide on Rheology and Tensile Properties. *Journal of Reinforced Plastics and Composites* **2001,** *20*, (8), 697-717.
37. de Carvalho Oliveira, G.; Filho, G. R.; Vieira, J. G.; De Assunção, R. M. N.; da Silva Meireles, C.; Cerqueira, D. A.; de Oliveira, R. J.; Silva, W. G.; de Castro Motta, L. A., Synthesis and application of methylcellulose extracted from waste newspaper in CPV-ARI Portland cement mortars. *J. Appl. Polym. Sci.* **2010,** *118*, (3), 1380-1385.
38. Abushammala, H.; Mao, J., A Review of the Surface Modification of Cellulose and Nanocellulose Using Aliphatic and Aromatic Mono- and Di-Isocyanates. *Molecules* **2019,** *24*, (15), 2782.
39. Jianlong, W.; Lujun, C.; Hanchang, S.; Yi, Q., Microbial degradation of phthalic acid esters under anaerobic digestion of sludge. *Chemosphere* **2000,** *41*, (8), 1245-1248.
40. Liu, S.; Suflita, J. M., Anaerobic biodegradation of methyl esters by Acetobacterium woodii and Eubacterium limosum. *Journal of Industrial Microbiology* **1994,** *13*, (5), 321-327.

41. Reese, E. T.; Siu, R. G. H.; Levinson, H. S., The biological degradation of soluble cellulose derivatives and its relationship to the mechanism of cellulose hydrolysis. *Journal of bacteriology* **1950,** *59*, (4), 485-497.
42. Vaca-Garcia, C.; Borredon, M. E.; Gaseta, A., Determination of the degree of substitution (DS) of mixed cellulose esters by elemental analysis. *Cellulose* **2001,** *8*, (3), 225-231.
43. Samaranayake, G.; Glasser, W. G., Cellulose derivatives with low DS. I. A novel acylation system. *Carbohydr. Polym.* **1993,** *22*, (1), 1-7.
44. King, A. W. T.; Jalomäki, J.; Granström, M.; Argyropoulos, D. S.; Heikkinen, S.; Kilpeläinen, I., A new method for rapid degree of substitution and purity determination of chloroform-soluble cellulose esters, using 31P NMR. *Anal. Methods* **2010,** *2*, (10), 1499-1505.
45. Blanchard, F. A.; Takahashi, I. T.; Alexander, H. C., Biodegradability of [14C]methylcellulose by activated sludge. *Appl. Environ. Microbiol.* **1976,** *32*, (4), 557-560.
46. Wirick, M. G., A study of the enzymic degradation of CMC and other cellulose ethers. *Journal of Polymer Science Part A-1: Polymer Chemistry* **1968,** *6*, (7), 1965-1974.
47. Wirick, M. G., Aerobic Biodegradation of Carboxymethylcellulose. *Journal (Water Pollution Control Federation)* **1974,** *46*, (3), 512-521.
48. Rivard, C. J.; Adney, W. S.; Himmel, M. E.; Mitchell, D. J.; Vinzant, T. B.; Grohmann, K.; Moens, L.; Chum, H., Effects of natural polymer acetylation on the anaerobic bioconversion to methane and carbon dioxide. *Applied Biochemistry and Biotechnology* **1992,** *34*, (1), 725-736.
49. Glasser, W. G.; McCartney, B. K.; Samaranayake, G., Cellulose derivatives with a low degree of substitution. 3. The biodegradability of cellulose esters using a simple enzyme assay. *Biotechnology Progress* **1994,** *10*, (2), 214-219.
50. Owen, W. F.; Stuckey, D. C.; Healy, J. B.; Young, L. Y.; McCarty, P. L., Bioassay for Monitoring Biochemical Methane Potential and Anaerobic Toxicity. *Water Res.* **1979,** *13*, (6), 485-492.
51. Hayakawa, C.; Funakawa, S.; Fujii, K.; Kadono, A.; Kosaki, T., Effects of climatic and soil properties on cellulose decomposition rates in temperate and tropical forests. *Biology and Fertility of Soils* **2014,** *50*, (4), 633-643.
52. Hofsten, B. V.; Edberg, N., Estimating the Rate of Degradation of Cellulose Fibers in Water. *Oikos* **1972,** *23*, (1), 29-34.
53. Goodwin, D. G.; Marsh, K. M.; Sosa, I. B.; Payne, J. B.; Gorham, J. M.; Bouwer, E. J.; Fairbrother, D. H., Interactions of Microorganisms with Polymer Nanocomposite Surfaces Containing Oxidized Carbon Nanotubes. *Environ. Sci. Technol.* **2015,** *49*, (9), 5484-5492.
54. Zhao, X.; Cornish, K.; Vodovotz, Y., Narrowing the Gap for Bioplastic Use in Food Packaging: An Update. *Environ. Sci. Technol.* **2020**.
55. Chinaglia, S.; Tosin, M.; Degli-Innocenti, F., Biodegradation rate of biodegradable plastics at molecular level. *Polym. Degrad. Stab* **2018,** *147*, 237-244.
56. Tokiwa, Y.; Calabia, B. P.; Ugwu, C. U.; Aiba, S., Biodegradability of plastics. *Int J Mol Sci* **2009,** *10*, (9), 3722-3742.
57. Artzi, L.; Bayer, E. A.; Moraïs, S., Cellulosomes: bacterial nanomachines for dismantling plant polysaccharides. *Nature Reviews Microbiology* **2017,** *15*, (2), 83-95.
58. Fierobe, H.-P.; Bayer, E. A.; Tardif, C.; Czjzek, M.; Mechaly, A.; Bélaïch, A.; Lamed, R.; Shoham, Y.; Bélaïch, J.-P., Degradation of Cellulose Substrates by Cellulosome Chimeras: Substrate Targeting Versus Proximity Of Enzyme Components. *Journal of Biological Chemistry* **2002,** *277*, (51), 49621-49630.
59. Wang, Z.-W.; Lee, S.-H.; Elkins, J. G.; Morrell-Falvey, J. L., Spatial and temporal dynamics of cellulose degradation and biofilm formation by Caldicellulosiruptor obsidiansis and Clostridium thermocellum. *AMB Express* **2011,** *1*, 30-30.
60. Ioelovich, M., Cellulose as a Nanostructured Polymer: A Short Review. *2008* **2008,** *3*, (4), 16.
61. Ioelovich, M., Characterization of Various Kinds of Nanocellulose. In *Handbook of Nanocellulose and Cellulose Nanocomposites*, 2017; pp 51-100.

62. Wang, Y.; Wang, X.; Xie, Y.; Zhang, K., Functional nanomaterials through esterification of cellulose: a review of chemistry and application. *Cellulose* **2018,** *25*, (7), 3703-3731.
63. Willberg-Keyriläinen, P.; Ropponen, J., Evaluation of esterification routes for long chain cellulose esters. *Heliyon* **2019,** *5*, (11), e02898.
64. Berlioz, S.; Molina-Boisseau, S.; Nishiyama, Y.; Heux, L., Gas-Phase Surface Esterification of Cellulose Microfibrils and Whiskers. *Biomacromolecules* **2009,** *10*, (8), 2144-2151.
65. Fumagalli, M.; Sanchez, F.; Boisseau, S. M.; Heux, L., Gas-phase esterification of cellulose nanocrystal aerogels for colloidal dispersion in apolar solvents. *Soft Matter* **2013,** *9*, (47), 11309-11317.
66. David, G.; Gontard, N.; Guerin, D.; Heux, L.; Lecomte, J.; Molina-Boisseau, S.; Angellier-Coussy, H., Exploring the potential of gas-phase esterification to hydrophobize the surface of micrometric cellulose particles. *Eur. Polym. J.* **2019,** *115*, 138-146.
67. Eyley, S.; Thielemans, W., Surface modification of cellulose nanocrystals. *Nanoscale* **2014,** *6*, (14), 7764-7779.
68. Peydecastaing, J.; Vaca-Garcia, C.; Borredon, E., Accurate determination of the degree of substitution of long chain cellulose esters. *Cellulose* **2008,** *16*, (2), 289.
69. Söyler, Z.; Meier, M. A. R., Sustainable functionalization of cellulose and starch with diallyl carbonate in ionic liquids. *Green Chem.* **2017,** *19*, (16), 3899-3907.
70. Zheng, Y.; Song, J.; Cheng, B.; Fang, X.; Yuan, Y., Preparation and flame retardancy of 3-(hydroxyphenylphosphinyl)-propanoic acid esters of cellulose and their fibers. *Cellulose* **2015,** *22*, (1), 229-244.
71. Willberg-Keyriläinen, P.; Orelma, H.; Ropponen, J., Injection Molding of Thermoplastic Cellulose Esters and Their Compatibility with Poly(Lactic Acid) and Polyethylene. *Materials (Basel)* **2018,** *11*, (12), 2358.
72. Son, D.; Cho, S.; Nam, J.; Lee, H.; Kim, M., X-ray-Based Spectroscopic Techniques for Characterization of Polymer Nanocomposite Materials at a Molecular Level. *Polymers* **2020,** *12*, (5), 1053.
73. Espino-Perez, E.; Domenek, S.; Belgacem, N.; Sillard, C.; Bras, J., Green Process for Chemical Functionalization of Nanocellulose with Carboxylic Acids. *Biomacromolecules* **2014,** *15*, (12), 4551-4560.
74. Langley, L. A.; Villanueva, D. E.; Fairbrother, D. H., Quantification of Surface Oxides on Carbonaceous Materials. *Chemistry of Materials* **2006,** *18*, (1), 169-178.
75. Shim, S. H.; Kim, K. T.; Lee, J. U.; Jo, W. H., Facile Method to Functionalize Graphene Oxide and Its Application to Poly(ethylene terephthalate)/Graphene Composite. *ACS Appl. Mater. Interfaces* **2012,** *4*, (8), 4184-4191.
76. Singh, M.; Kaushik, A.; Ahuja, D., Surface functionalization of nanofibrillated cellulose extracted from wheat straw: Effect of process parameters. *Carbohydr. Polym.* **2016,** *150*, 48-56.
77. Braun, E. I.; Pantano, P., The importance of an extensive elemental analysis of single-walled carbon nanotube soot. *Carbon* **2014,** *77*, 912-919.
78. Bohutskyi, P.; Betenbaugh, M. J.; Bouwer, E. J., The effects of alternative pretreatment strategies on anaerobic digestion and methane production from different algal strains. *Bioresource Technology* **2014,** *155*, 366-372.
79. Dai, X.; Chen, Y.; Zhang, D.; Yi, J., High-solid Anaerobic Co-digestion of Sewage Sludge and Cattle Manure: The Effects of Volatile Solid Ratio and pH. *Sci. Rep.* **2016,** *6*, (1), 35194.
80. Mei, R.; Narihiro, T.; Nobu, M. K.; Kuroda, K.; Liu, W.-T., Evaluating digestion efficiency in full-scale anaerobic digesters by identifying active microbial populations through the lens of microbial activity. *Sci. Rep.* **2016,** *6*, (1), 34090.
81. Yi, J.; Dong, B.; Jin, J.; Dai, X., Effect of increasing total solids contents on anaerobic digestion of food waste under mesophilic conditions: performance and microbial characteristics analysis. *PloS one* **2014,** *9*, (7), e102548-e102548.
82. Koch, K.; Hafner, S. D.; Astals, S.; Weinrich, S., Evaluation of Common Supermarket Products as Positive Controls in Biochemical Methane Potential (BMP) Tests. *Water* **2020,** *12*, (5), 1223.

83. Bohutskyi, P.; Keller, T. A.; Phan, D.; Parris, M. L.; Li, M.; Richardson, L.; Kopachevsky, A. M., Co-digestion of Wastewater-Grown Filamentous Algae With Sewage Sludge Improves Biomethane Production and Energy Balance Compared to Thermal, Chemical, or Thermochemical Pretreatments. *Frontiers in Energy Research* **2019,** *7*, (47).
84. Li, P.; Li, W.; Sun, M.; Xu, X.; Zhang, B.; Sun, Y., Evaluation of Biochemical Methane Potential and Kinetics on the Anaerobic Digestion of Vegetable Crop Residues. *Energies* **2019,** *12*, (1), 26.
85. Yan, H.; Zhao, C.; Zhang, J.; Zhang, R.; Xue, C.; Liu, G.; Chen, C., Study on biomethane production and biodegradability of different leafy vegetables in anaerobic digestion. *AMB Express* **2017,** *7*, (1), 27.
86. Lakhundi, S.; Siddiqui, R.; Khan, N. A., Cellulose degradation: a therapeutic strategy in the improved treatment of Acanthamoeba infections. *Parasites & Vectors* **2015,** *8*, (1), 23.
87. Note: dodecyl ester CNF and DA-CNF-2 are the same sample used in two different data sets.
88. Homma, I.; Fukuzumi, H.; Saito, T.; Isogai, A., Effects of carboxyl-group counter-ions on biodegradation behaviors of TEMPO-oxidized cellulose fibers and nanofibril films. *Cellulose* **2013,** *20*, (5), 2505-2515.
89. Homma, I.; Isogai, T.; Saito, T.; Isogai, A., Degradation of TEMPO-oxidized cellulose fibers and nanofibrils by crude cellulase. *Cellulose* **2013,** *20*, (2), 795-805.
90. Haske-Cornelius, O.; Pellis, A.; Tegl, G.; Wurz, S.; Saake, B.; Ludwig, R.; Sebastian, A.; Nyanhongo, G. S.; Guebitz, G. M., Enzymatic Systems for Cellulose Acetate Degradation. *Catalysts* **2017,** *7*, (10), 287.
91. White, G. F.; Russell, N. J.; Tidswell, E. C., Bacterial scission of ether bonds. *Microbiol Rev* **1996,** *60*, (1), 216-232.
92. Teeri, T. T., Crystalline cellulose degradation: new insight into the function of cellobiohydrolases. *Trends in Biotechnology* **1997,** *15*, (5), 160-167.
93. Johansson, L.-S.; Tammelin, T.; Campbell, J. M.; Setala, H.; Osterberg, M., Experimental evidence on medium driven cellulose surface adaptation demonstrated using nanofibrillated cellulose. *Soft Matter* **2011,** *7*, (22), 10917-10924.
94. Cumpstey, I., Chemical modification of polysaccharides. *ISRN Org Chem* **2013,** *2013*, 417672-417672.
95. Heinze, T.; El Seoud, O. A.; Koschella, A., *Cellulose Derivatives: Synthesis, Structure, and Properties*. Springer International Publishing: Switzerland, 2018.
96. Huang, F.-Y., Thermal Properties and Thermal Degradation of Cellulose Tri-Stearate (CTs). *Polymers* **2012,** *4*, (2), 1012-1024.
97. Vaca-Garcia, C.; Thiebaud, S.; Borredon, M. E.; Gozzelino, G., Cellulose esterification with fatty acids and acetic anhydride in lithium chloride/N,N-dimethylacetamide medium. *Journal of the American Oil Chemists' Society* **1998,** *75*, (2), 315-319.
98. Okazaki, M.; Moo-Young, M., Kinetics of enzymatic hydrolysis of cellulose: Analytical description of a mechanistic model. *Biotechnology and Bioengineering* **1978,** *20*, (5), 637-663.
99. Gaikwad, A., Effect of Particle Size on the Kinetics of Enzymatic Hydrolysis of Microcrystalline Cotton Cellulose: a Modeling and Simulation Study. *Applied Biochemistry and Biotechnology* **2019,** *187*, (3), 800-816.
100. Vickerman, J. C.; GIlmore, I. S., *Surface Analysis: The Principal Techniques*. Second ed.; Wiley: 2009.
101. Petersen, E. J.; Zhang, L.; Mattison, N. T.; O'Carroll, D. M.; Whelton, A. J.; Uddin, N.; Nguyen, T.; Huang, Q.; Henry, T. B.; Holbrook, R. D.; Chen, K. L., Potential Release Pathways, Environmental Fate, And Ecological Risks of Carbon Nanotubes. *Environ. Sci. Technol.* **2011,** *45*, (23), 9837-9856.
102. Bai, Y.; Wu, F.; Lin, D.; Xing, B., Aqueous stabilization of carbon nanotubes: effects of surface oxidization and solution chemistry. *Environmental Science and Pollution Research* **2014,** *21*, (6), 4358-4365.

103. Frank, B. P.; Sigmon, L. R.; Deline, A. R.; Lankone, R. S.; Gallagher, M. J.; Zhi, B.; Haynes, C. L.; Fairbrother, D. H., Photochemical Transformations of Carbon Dots in Aqueous Environments. *Environ. Sci. Technol.* **2020,** *54*, (7), 4160-4170.
104. Zhang, B.; Liu, C.-y.; Liu, Y., A Novel One-Step Approach to Synthesize Fluorescent Carbon Nanoparticles. *European Journal of Inorganic Chemistry* **2010,** *2010*, (28), 4411-4414.
105. Zhao, P.; Zhu, L., Dispersibility of carbon dots in aqueous and/or organic solvents. *Chemical Communications* **2018,** *54*, (43), 5401-5406.
106. Nuncira, J.; Seara, L. M.; Sinisterra, R. D.; Caliman, V.; Silva, G. G., Long-term colloidal stability of graphene oxide aqueous nanofluids. *Fullerenes, Nanotubes and Carbon Nanostructures* **2019**, 1-11.
107. Qi, Y.; Xia, T.; Li, Y.; Duan, L.; Chen, W., Colloidal stability of reduced graphene oxide materials prepared using different reducing agents. *Environ. Sci.: Nano* **2016,** *3*, (5), 1062-1071.
108. Baker, A. A.; Helbert, W.; Sugiyama, J.; Miles, M. J., New Insight into Cellulose Structure by Atomic Force Microscopy Shows the Iα Crystal Phase at Near-Atomic Resolution. *Biophys J* **2000,** *79*, (2), 1139-1145.
109. Stern, J.; Moraïs, S.; Lamed, R.; Bayer, E. A., Adaptor Scaffoldins: An Original Strategy for Extended Designer Cellulosomes, Inspired from Nature. *mBio* **2016,** *7*, (2), e00083-16.
110. Wang, Y.; Leng, L.; Islam, M. K.; Liu, F.; Lin, C. S. K.; Leu, S.-Y., Substrate-Related Factors Affecting Cellulosome-Induced Hydrolysis for Lignocellulose Valorization. *Int J Mol Sci* **2019,** *20*, (13), 3354.
111. Aulin, C.; Ahola, S.; Josefsson, P.; Nishino, T.; Hirose, Y.; Österberg, M.; Wågberg, L., Nanoscale Cellulose Films with Different Crystallinities and Mesostructures—Their Surface Properties and Interaction with Water. *Langmuir* **2009,** *25*, (13), 7675-7685.
112. Ahola, S.; Salmi, J.; Johansson, L. S.; Laine, J.; Österberg, M., Model Films from Native Cellulose Nanofibrils. Preparation, Swelling, and Surface Interactions. *Biomacromolecules* **2008,** *9*, (4), 1273-1282.
113. Spence, K. L.; Venditti, R. A.; Rojas, O. J.; Habibi, Y.; Pawlak, J. J., The effect of chemical composition on microfibrillar cellulose films from wood pulps: water interactions and physical properties for packaging applications. *Cellulose* **2010,** *17*, (4), 835-848.
114. Westerholm, M.; Schnurer, A., Microbial Responses to Different Operating Practices for Biogas Production Systems. In *Anaerobic Digestion*, Banu, R., Ed. IntechOpen: 2019.
115. Mahamat, A. Y.; Gourdon, R.; Leger, P.; Vermande, P., Methane recovery by anaerobic digestion of cellulosic materials available in Sahel. *Biological Wastes* **1989,** *30*, (3), 181-197.
116. Komarek, R. J.; Gardner, R. M.; Buchanan, C. M.; Gedon, S., Biodegradation of radiolabeled cellulose acetate and cellulose propionate. *J. Appl. Polym. Sci.* **1993,** *50*, (10), 1739-1746.
117. Wei, L.; Agarwal, U. P.; Hirth, K. C.; Matuana, L. M.; Sabo, R. C.; Stark, N. M., Chemical modification of nanocellulose with canola oil fatty acid methyl ester. *Carbohydr. Polym.* **2017,** *169*, 108-116.
118. Ferreira, F. V.; Pinheiro, I. F.; Gouveia, R. F.; Thim, G. P.; Lona, L. M. F., Functionalized cellulose nanocrystals as reinforcement in biodegradable polymer nanocomposites. *Polym. Compos.* **2018,** *39*, (S1), E9-E29.
119. Kargarzadeh, H.; Huang, J.; Lin, N.; Ahmad, I.; Mariano, M.; Dufresne, A.; Thomas, S.; Gałęski, A., Recent developments in nanocellulose-based biodegradable polymers, thermoplastic polymers, and porous nanocomposites. *Progress in Polymer Science* **2018,** *87*, 197-227.
120. Mishra, R. K.; Sabu, A.; Tiwari, S. K., Materials chemistry and the futurist eco-friendly applications of nanocellulose: Status and prospect. *Journal of Saudi Chemical Society* **2018,** *22*, (8), 949-978.
121. Rodionova, G.; Lenes, M.; Eriksen, Ø.; Gregersen, Ø., Surface chemical modification of microfibrillated cellulose: improvement of barrier properties for packaging applications. *Cellulose* **2011,** *18*, (1), 127-134.

122. Yagyu, H.; Ifuku, S.; Nogi, M., Acetylation of optically transparent cellulose nanopaper for high thermal and moisture resistance in a flexible device substrate. *Flexible and Printed Electronics* **2017,** *2*, (1), 014003.
123. Yang, S.; Xie, Q.; Liu, X.; Wu, M.; Wang, S.; Song, X., Acetylation improves thermal stability and transmittance in FOLED substrates based on nanocellulose films. *RSC Adv.* **2018,** *8*, (7), 3619-3625.
124. Barhoum, A.; Samyn, P.; Öhlund, T.; Dufresne, A., Review of recent research on flexible multifunctional nanopapers. *Nanoscale* **2017,** *9*, (40), 15181-15205.
125. Mertaniemi, H.; Laukkanen, A.; Teirfolk, J.-E.; Ikkala, O.; Ras, R. H. A., Functionalized porous microparticles of nanofibrillated cellulose for biomimetic hierarchically structured superhydrophobic surfaces. *RSC Adv.* **2012,** *2*, (7), 2882-2886.
126. Zhang, Y.; Wei, L.; Hu, H.; Zhao, Z.; Huang, Z.; Huang, A.; Shen, F.; Liang, J.; Qin, Y., Tribological properties of nano cellulose fatty acid esters as ecofriendly and effective lubricant additives. *Cellulose* **2018,** *25*, (5), 3091-3103.

957

a)

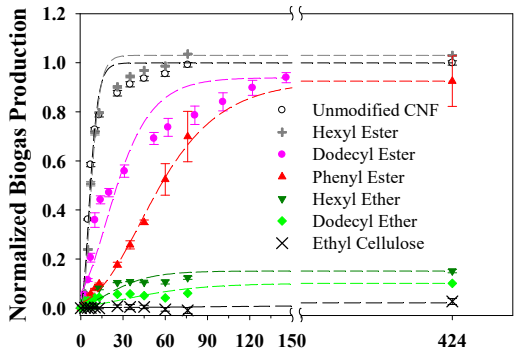

b)

Sample	$DS_{surface}$	$DS_{overall}$	Normalized K	Normalized V_{max}
Unmodified CNF	0	0	0.078	1.01
Hexyl Ester CNF	0.030	0.09	0.095	1.03
Phenyl Ester CNF	0.17	0.14	0.011	0.93
Dodecyl Ester CNF	0.097	0.45	0.020	0.94
Dodecyl Ether CNF	0.16	0.11	0.0010	0.10
Hexyl Ether CNF	0.25	0.05	0.0030	0.15
Na^+ Carboxyl CNF	-	0.24	0.016	0.85
H^+ Carboxyl CNF	-	0.24	0.020	0.87

c)

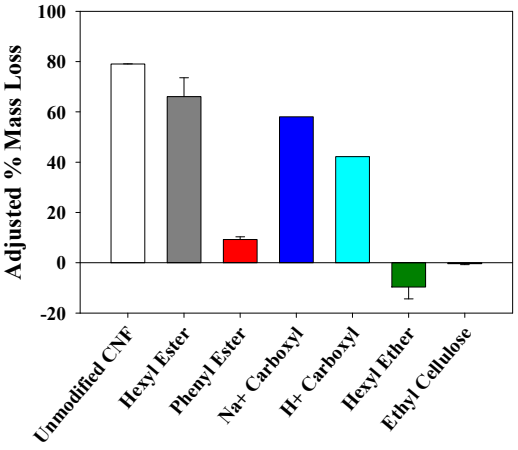

d)

Sample	Biodegradation Relative to Unmodified CNF	
	Anaerobic	Aerobic
Unmodified CNF	1.00 ± 0.01	1.000 ± 0.001
Hexyl Ester CNF	1.033 ± 0.003	0.84 ± 0.09
Phenyl Ester CNF	0.55 ± 0.07	0.12 ± 0.01
Na+ Carboxyl CNF	0.75	0.73
H+ Carboxyl CNF	0.83	0.53
Hexyl Ether CNF	0.111 ± 0.009	-0.12 ± 0.06
Ethyl Cellulose	-0.005 ± 0.008	-0.004 ± 0.005

Figure 1. Anaerobic and aerobic biodegradation of functionalized cellulose nanofibrils (CNF). a) Normalized biogas production by an anaerobic microbial community degrading the indicated CNFs as a function of incubation time (dodecyl ester CNF was not sampled past 146 days). For each sample, values are normalized to the maximum calculated biogas produced by both cellulose and the added functional group (see text for details). Error bars represent one standard deviation from duplicate samples. b) $DS_{surface}$ and $DS_{overall}$ values determined by XPS and elemental analysis, respectively and K and V_{max} derived from modified Gompertz model fitting of biodegradation data for functionalized CNFs. c) Mass loss at 60 d for degradation of the indicated CNFs by an aerobic microbial community. Values shown represent the difference between microbial and blank samples (see experimental section for details). Error bars represent one standard deviation from duplicate samples. Na^+ and H^+ Carboxyl CNF samples were not run in duplicate due to limitations in sample mass. d) Comparison of the inhibition of biodegradation for different functionalized CNFs in anaerobic vs. aerobic environments relative to unmodified CNF.

958

959

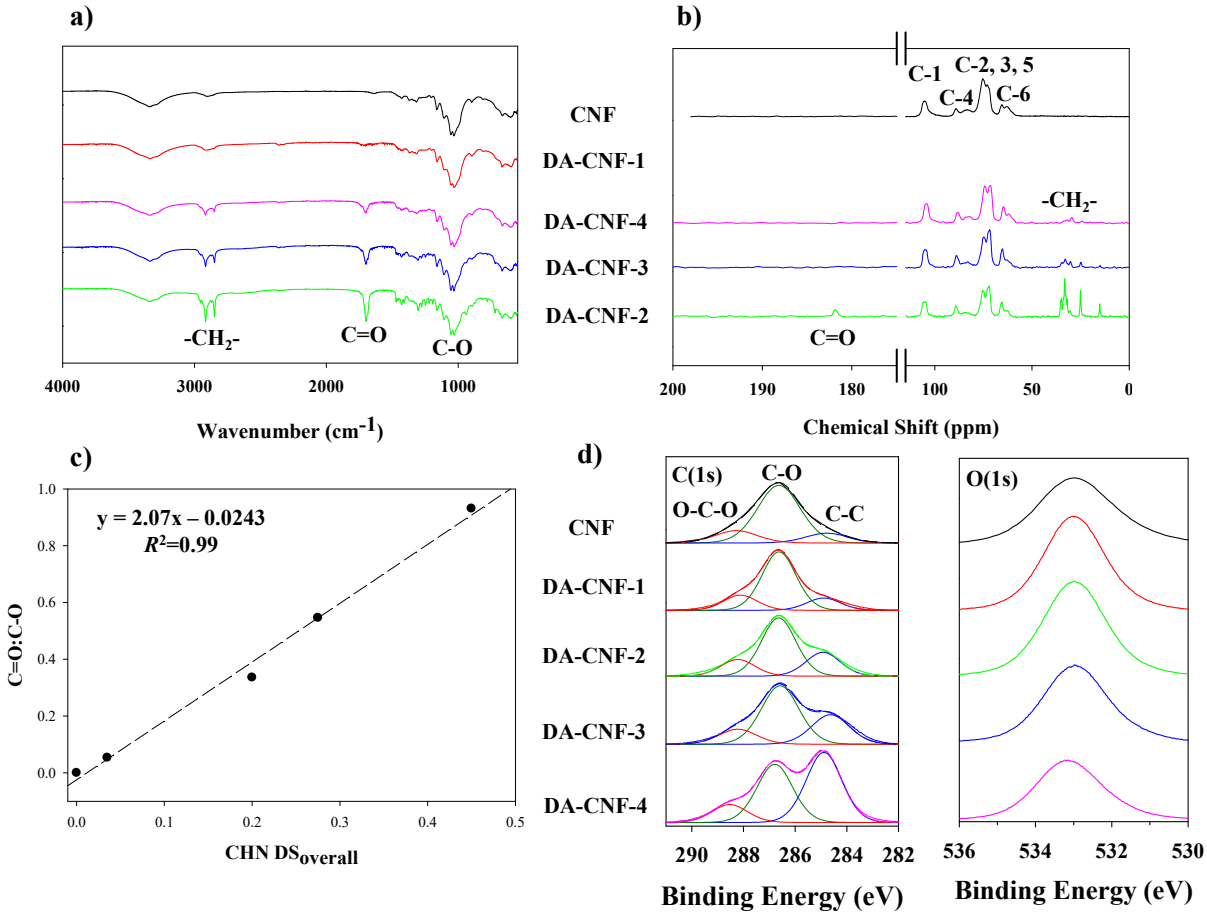

Figure 2. Characterization of esterified cellulose nanofibrils (CNFs). a) Attenuated total reflectance Fourier transform infrared spectroscopy (ATR-FTIR) of unmodified CNF (black), and DA-CNF-1 (red), DA-CNF-4 (pink), DA-CNF-3 (blue), and DA-CNF-2 (green) dodecyl ester CNFs. The unmodified CNF contains the characteristic O–H (3339 cm^{-1}), C–H (2905 cm^{-1}), and C–O (1031 cm^{-1}) stretches of cellulose with CH_2 and C=O peaks due to the ester linkages b) Solid-state ^{13}C-NMR spectra of unmodified CNFs (black), DA-CNF-4 (pink), DA-CNF-3 (blue), and DA-CNF-2 (green) dodecyl ester CNFs. c) Relation between vibrational peak ratio (C=O:C–O) and overall DS calculated from CHN elemental analysis %C data. d) X-ray photoelectron C(1s) and O(1s) spectra of unmodified CNFs (black), DA-CNF-1 (red), DA-CNF-2 (green), DA-CNF-3 (blue), and DA-CNF-4 (pink) dodecyl ester CNFs.

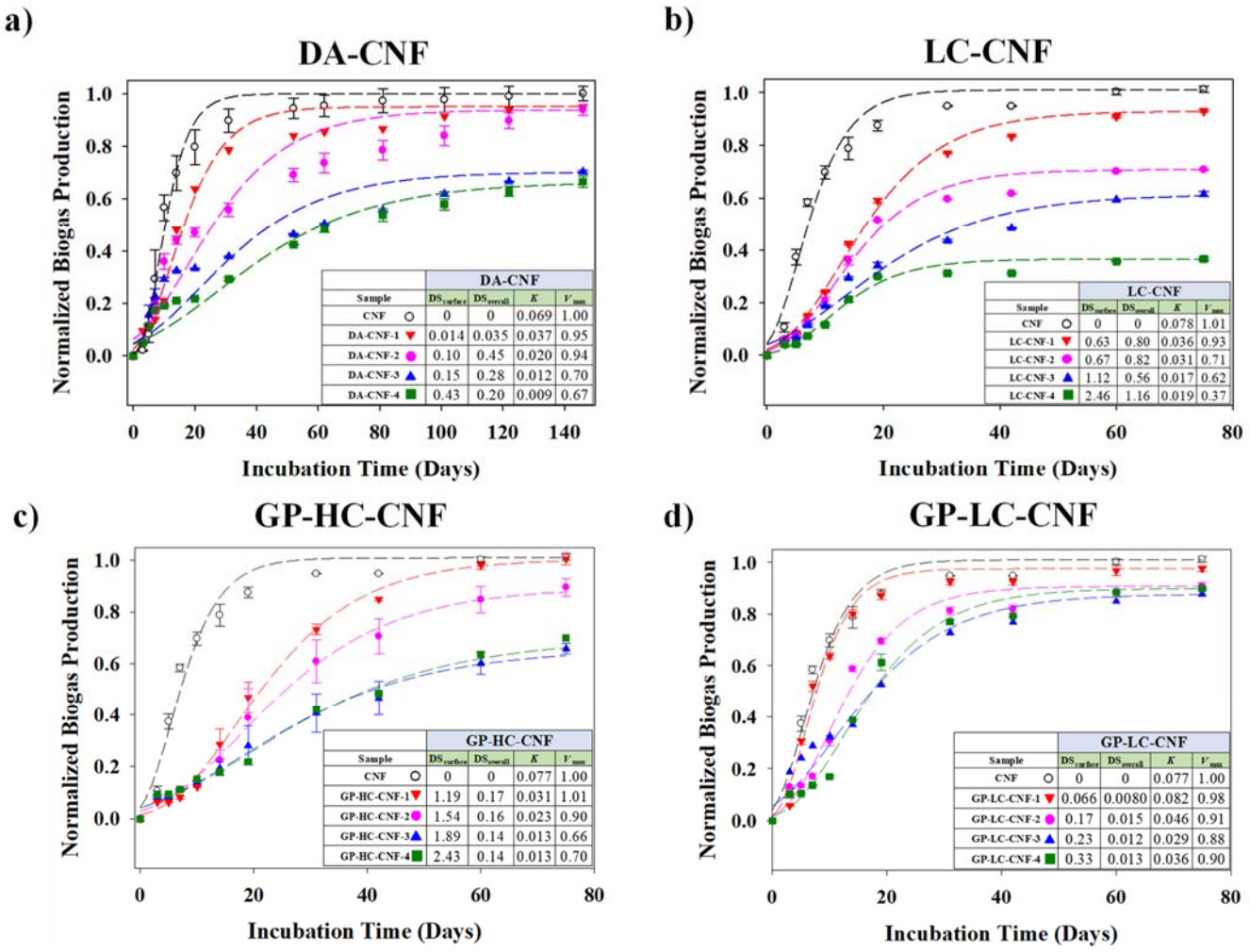

Figure 3. Biogas production and modified Gompertz model fits (dotted lines) of cellulose nanofibrils (CNFs) esterified using liquid- and gas-phase methods. Relative biogas production from cellulose nanofibrils esterified using a) liquid-phase dodecanoic acid (DA-CNF), b) liquid-phase lauroyl chloride (LC-CNF), c) gas-phase hexanoyl chloride (GP-HC-CNF), and d) gas-phase lauroyl chloride (GP-LC-CNF). Biogas volumes are normalized to the maximum calculated biogas production expected from the combined cellulose and functional group components of each sample (Table S4). The $DS_{surface}$ and $DS_{overall}$ values, as well as normalized maximum biogas volume (V_{max}) and biogas production rate (K) for each sample are provided in the inset of each plot. Accuracy for Gompertz parameters is reported in Table S5.